Journal of Drug Delivery Science and Technology 57 (2020) 101741

Contents lists available at ScienceDirect

Journal of Drug Delivery Science and Technology

journal homepage: www.elsevier.com/locate/jddst

Hyperbranched polyglycerol β-cyclodextrin as magnetic platform for optimization of doxorubicin cytotoxic effects on Saos-2 bone cancerous cell line

Nafiseh Khelghati[a], Yousef Rasmi[a,b,*], Navid Farahmandan[c], Alireza Sadeghpour[c], Seyed Mostafa Mir[c], Ansar Karimian[c], Bahman Yousefi[d,**]

[a] Department of Biochemistry, Faculty of Medicine, Urmia University of Medical Sciences, Urmia, Iran
[b] Cellular and Molecular Research Center, Urmia University of Medical Sciences, Urmia, Iran
[c] Drug Applied Research Center, Tabriz University of Medical Sciences, Tabriz, Iran
[d] Molecular Medicine Research Center, Tabriz University of Medical Sciences, Tabriz, Iran

ARTICLE INFO

Keywords:
β-Cyclodextrin
Targeted delivery
Doxorubicin
Magnetic nanoparticles
Saos-2 cell line
Bone cancer

ABSTRACT

In recent years, cancer has become the most important human health problems in the world. To overcome these problems, chemotherapy as a treatment approach is widely used in cancer treatment. However, single chemotherapy have a toxic side effects without completely effectiveness. This study has focused on the mitigating of doxorubicin side effects by designing pH-sensitive magnetic hyperbranched β-cyclodextrin as a nano-sized drug carrier. The accuracy of samples preparation has been confirmed by several characterizations including FTIR, NMR, SEM, EDX, TEM, XRD, DLS and Zeta Potential tests. The hemolysis assay results have shown that synthesized nanocarrier is completely biocompatible and could be used in blood contacting applications. In this case, nanoparticles have a better release in acidic pH value. *In-vitro* studies including MTT assay uptake assay, DAPI staining and apoptosis assay by flow-cytometry have been carried out on Saos-2 cell line. It is concluded that a synthesized doxorubicin-loaded nanocarrier has more cytotoxicity than free doxorubicin after incubation time, showing its high potentiality for target doxorubicin delivery to Saos-2 cell line.

1. Introduction

Cancer is globally converted to one of the biggest public health challenges [1] as the second most common concern(s) caused death in developed and developing countries [2,3]. Considering many types of cancers, osteosarcoma is a malignant and invasive neoplasm derived from bone marrow mesenchymal cells that occurs in children and adolescents [4,5]. Surgery, radiotherapy and chemotherapy are among the standard selective treatments for osteosarcoma [6,7]. Despite the common use of chemotherapy in cancer treatment, chemotherapeutic agent side effects have confined its usage(s). Doxorubicin (DOX) or Adriamycin as a chemotherapy medication with a range of antitumor and anticancer activities is used in cancer patients whether children or adolescents as well as osteosarcoma [8]. The main mechanisms is the interaction aromatic part of DOX with DNA and inhibiting cell proliferation [9,10]. One of the main DOX side effects is dose-dependent cardio and hepatotoxicity due to oxidative stress, DNA damage, production of reactive oxygen species (ROS), and creating multi-drug resistance (MDR) [11–13]. Drug delivery systems (DDSs) are the appropriate mechanism for reducing the side effects of chemotherapeutic agents and enhanced permeability and retention effect (EPR), resulting the accumulation of drugs in cancerous tissue [14–16]. DDSs also make the lowest dose of chemotherapy agent transformation to the exact location of tumor with no harm to healthy tissue [17]. An ideal DDSs feature is biocompatible, biodegradability, least effect on the immune system, minimum hemolytic effect on blood, predictable control release of drugs in target tissue and predictable systemic clearness [18]. In this regard, numerous systems have been used to delivery of drugs with smart properties such as liposome, micelles, dendrimer, polymer and nanoparticles and have attracted much attention in recent years [19–22]. At the meantime, nanoparticles that can respond to different stimuli such as light, temperature, ultrasound, magnetic field, enzyme, pH, and oxidative-reduction can be well-guided to target tissue [23–25]. Gold, silver, zinc, and titanium are widely used in biomedical

* Corresponding author. Department of Biochemistry, Faculty of Medicine, Urmia university of Medical Sciences, Urmia, Iran.
** Corresponding author. Molecular Medicine Research Center, Tabriz University of Medical Sciences, Tabriz, Iran.
E-mail addresses: rasmiy@umsu.ac.ir (Y. Rasmi), bahmanusefi@gmail.com (B. Yousefi).

https://doi.org/10.1016/j.jddst.2020.101741
Received 14 February 2020; Received in revised form 2 April 2020; Accepted 7 April 2020
Available online 20 April 2020
1773-2247/

application with various purposes [26–29]. However, using iron oxide magnetic nanoparticles (Fe_3O_4) is an excellent platform for DDSs to guide the drug toward the target tissue while assisted by an external magnetic field [30]. The unique properties of Fe_3O_4 are its superparamagnetic behavior, small size, high half-life, low toxicity, hydrophilic nature, high free energy and the ability to rapid decomposition and disinfection from body [31,32]. Despite this advantages, some challenges are seen such as tendency to accumulate in aqueous solutions, phagocytosis and removal by renal filtrations and reticuloendothelial system, and limiting the use of magnetic nanoparticles in clinical trials [33]. However, the use of stabilizers such as hydrophilic polymer to cover the surface of nanoparticles could increase stability, hydrophilicity, biodegradability, dispersion and escaping from phagocytosis [34,35]. Cyclodextrin is a very stable cyclic macrocycle including the binding of 6, 7 or 8 molecules of glucose called α, β and γ-cyclodextrin [36]. Cyclodextrin has a hydrophilic surface and a hydrophobic cavity with several hydroxyl functional groups [37]. Features such as being natural, renewable, biodegradability, biocompatibility, proper interactions, good operating efficiency and hydrophilicity have made this compound suitable for use in biomedical applications [38]. By grafting several active groups such as amine, carboxylic acid, and poly-hydroxyl, it can be converted to more active platform to link and connect with target tissue in DDSs [39–41]. For example, polyglycerol section could improve the therapeutic effectiveness of drug carrier due to the greater stability, improved blood circulation time, improved biodistribution, and improved tumor penetration. Thus, grafting of hyperbranched polyglycerol could improve the cyclodextrin carrier properties. In this study, hyperbranched cyclodextrin with a core of Fe_3O_4 nanoparticle to deliver DOX as chemotherapeutic agent to Saos-2 bone cancer cells are chosen. Physical and chemical properties of synthetic nanomaterials such as particle size and charge, particle surface morphology, and molecule structure are confirmed by using chemical techniques such as FTIR, NMR, TEM, SEM, EDX, XRD, DLS and Zeta Potential. The biocompatibility of nanocarriers is performed by hemolysis assay on human blood samples. *In-vitro* studies have been carried out on Saos-2 cell lines, and the growing efficacy ratio in drug has been confirmed by the use of nano-drugs with biological assays including uptake assay, apoptosis assay, DAPI staining and MTT assay.

2. Materials and methods

2.1. Materials

β-Cyclodextrin (β-CD, 98%), sodium hydride (NaH), sodium hydroxid (NaOH), glycidol, acetone, epichlorohydrin, dioxane, ferric chloride hexahydrate ($FeCl_3.6H_2O$), ferrous chloride tetrahydrate ($FeCl_2.4H_2O$), and 4′,6-diamidino-2-phenylindole (DAPI) are purchased from Sigma-Aldrich Co. Ammonia solution (28%), dimethylformamide (DMF), dimethylsulfoxide (DMSO), other solvents and all other chemical reagents are provided from Merck Co and used while received. Roswell Park Memorial Institute 1640 growth medium (RPMI), trypsin, and fetal bovine serum (FBS) are obtained from Gibco BRL Life Technologies. Doxorubicin powders are purchased Sobhan Pharmaceutical Co. 3-(4, 5- dimethylthiazol-2-yl)-2, 5-diphe-nyltetrazolium bromide (MTT) is provided from Bio Basic Co. Human red blood cells (HRBCs) are obtained from the Iranian Blood Transfusion Institute (IBTI) and become stable with ethylene diamine tetra acetic acid (EDTA). eBioscience™ Annexin V-FITC Apoptosis Detection Kit is obtained from Invitrogen Co.

2.2. Instrumentation

Fourier transform infrared (FTIR) spectroscopy: Chemical structures of samples are functioned with FTIR spectroscopy in a range of 500–4000 cm^{-1} by Bruker Tensor 270 spectrometer.

NMR: The nuclear magnetic resonance (NMR) spectroscopy (Bruker Co., Germany) is functioned to validate the chemical structure of prepared samples and deuterated DMSO used as a solvent.

Dynamic light scattering (DLS): average diameter of nanoparticles are determined by using laser-scattering techniques by Zetasizer Nano ZS90, Malvern Instruments, Malvern, UK. Therefore, based on prior analysis, samples are diluted by distilled water in concentration of 10 ppm.

Scanning electron microscopy (SEM) and energy dispersive X-ray (EDX): morphology, size, and elemental percentage analysis of samples are examined by using a Field Emission Scanning Electron Microscopy and Energy Dispersive X-ray (FESEM-EDX; S4160 Hitachi, Japan). Samples are attached to a metal stub by using a carbon double-sided adhesive tape and enclosed with a thin layer of gold by using a direct current sputter technique (Emitechk450X, England).

X-ray diffraction (XRD): Atomic and molecular structure of a crystal is examined with X-ray Rigaku Utma 4 diffractometer, power of 50 kV/50 mA and Cu Ka irradiation in an angle range (2θ) of 10–80° in ambient temperature. XRD is functioned X' Pert Pro, Malvern Panalytical Ltd (Almelo, Netherlands).

Transmission Electron Microscopy (TEM): Size and morphology of the samples are determined by electron microscopy CM120, Philips, Germany with operating at 200 kV. Before analysis, the suspension is ultrasonically dispersed by using a probe-type ultrasonic generator (400 W) for 6 s and the suspension is placed on a copper grid within 2 min.

2.3. Preparation of magnetic hyperbranched cyclodextrin

- *Preparation of hyperbranched polyglycerol modified β-cyclodextrin (HPG-β-CD)*: 0.8 gr (0.48 mmol) of dried β-CD is dissolved in 80 mL of DMF in a magnetic stirrer at 25 °C, which is followed by putting the solution in an ice bath and slowly adding 0.270 gr (6.72 mmol) NaH to a cold suspension to be stirred for 2 h. Subsequently, 0.249 gr (3.36 mmol) glycidol is dissolved in DMF and gradually added to the solution. The mixture is stirred for 48 h, then precipitate the solution as droplets to cold acetone in ice bath. Centrifuge (8000RPM, 15 min) separates the sediment from the solvent. With the help of a frizzed dryer, precipitate is completely dried in 24 h [42].
- *Preparation of magnetic nanocarrier*: 0.75 gr (2.77 mmol) $FeCl_3.6H_2O$ and 0.27 gr (1.38 mmol) $FeCl_2.4H_2O$ are dissolved in 25 mL distilled water. This solution is mixed and de-gased with the help of high-pressure nitrogen gas and stirred for 30 min. Then ammonia solution has been gradually added until solvent pH is reached to 10 and stirred for 45 min. Later, the centrifugation is used (7000 rpm, 15 min) for washing and purification for several times with deionized water and ethanol. The precipitate (Fe_3O_4 NPs) is completely dried in a freeze-drying method [19]. 0.24 gr NaOH is dissolved in 3.5 ml distilled water, then 0.4 ml 1.4-dioxane and 0.8 ml epichlorohydrine are added to this solution. 0.2 gr Fe_3O_4 is also added to the above solution and stirred for 4 h, then isolated by an external magnetic field and dried in vacuum condition. 30 mg of prepared Fe_3O_4 NPs is mixed in 2 ml PBS. By adding hydrochloric acid, pH of the solution has been adjusted to pH = 1 [43]. Afterwards, 60 mg of HPG-β-CD is added and vigorously stirred for 24 h. Finally, the HPG-β-CD modified with magnetic nanoparticles (HPG-β-CD/Fe_3O_4 NPs) has been obtained.

2.4. DOX loading in the magnetic nanocarrier

In order to load DOX in magnetic nanocarrier, 37.18 mg of magnetic nanocarrier is dispersed in 3.7 mg mL^{-1} DOX solution and stirred in ambient temperature in a sealed vial at darkness for 24 h. The supernatant is taken out by an external magnetic field, then the optical density of supernatant is measured by UV–Vis spectroscopy at 480 nm.

Draw a calibration curve of different concentration of free DOX and calculate the concentration of unloaded drug on the supernatant. Drug loading efficiency (DLE) and drug encapsulation efficiency (DEE) of DOX are calculated by the following formulas [44]:

$$\text{Drug Loading efficiency } (\% \frac{w}{w}) = \frac{\text{Mass of drug in nanocarrier}}{\text{Mass of the nanocarrier}} \times 100$$

$$\text{Drug encapsulation efficiency } (\% \frac{w}{w}) = \frac{\text{Mass of drug in nanocarrier}}{\text{Mass of drug}} \times 100$$

The obtained precipitate (DOX-nanocarrier) is washed with an appropriate amount of PBS and vacuumed dried for further *in-vitro* studies.

2.5. In vitro DOX release

Drug released from DOX-nanocarrier is evaluated in pH values of 4, 5.2 and 7.4 for simulated lysozyme, cancer tissue and physiological condition, respectively. For this purpose, 4 mg of DOX-nanocarrier is dispersed in 1 mL PBS solution with different pH values and shaken in incubator at 37 ºC. The supernatant is collected by using an external magnetic field after a predetermined time (1 h, 2 h, 4 h, 6 h,12 h, 24 h, 48 h,72 h, etc.). The absorbance of supernatant is measured by UV–Vis spectrophotometer (at 480 nm). By using the calibration curve of DOX, the absorbance of released DOX are converted to their concentration. Finally, the amount of drug release at any time is calculated by the following formula [44,45]:

$$\text{Drug release } (\%) = \frac{ammount\ of\ drug\ release\ in\ medium}{amount\ of\ drug\ loaded\ in\ nanocarrier} \times 100$$

2.6. Hemolysis assay

In order to evaluate the biocompatibility of synthesized nanocarrier, hemolysis assay test is performed [46]. In this regard, 1 ml of fresh human red blood cells (HRBCs) is stabilized with EDTA and washed 10 times with PBS until the supernatant of sample is clear (centrifugation at 2500 for 10 min). 0.5 ml of RBCs suspension is incubated with 0.5 ml of different concentration of nanocarrier (final concentrations of nanocarrier: 4000, 2000, 1000, 500, 250, 125, 62.5 and 31.25 μg mL^{-1}). Also, 0.5 ml of RBCs suspension is incubated with 0.5 ml deionized water, PBS solution as positive (100% hemolysis rate) and negative control (0% hemolysis rate), respectively. All samples are shaken at 37 ˚C for 4 h and centrifuged at 1000 rpm for 15 min. 200 μl of supernatant is transferred to a 96-well plate, and the absorbance value at 540 nm is measured by using an ELISA reader. Finally, the hemolysis rate is measured through this formula [19]:

$$\text{Hemolysis } (\%) = \frac{OD_{sample} - OD_{negative.c}}{OD_{Positive.c} - OD_{negative.c}} \times 100$$

2.7. Cell culture and in-vitro cytotoxicity assay

Cancerous Saos-2 cells are cultured in RPMI (contain penicillin-streptomycin) with 10% FBS and incubated 24 h in 37 ˚C. *in-vitro* cytotoxicity of nanocarrier, free DOX, and DOX-nanocarrier are performed against the Saos-2 cells through MTT assay [19]. In 96-well plates, 15,000 cells are seeded per well. In order to reach the volume of each well to 200 μl, an appropriate amount of growth medium with 10% FBS is added. Then, the plate is incubated at 37 ˚C in a humidified atmosphere with 5% CO_2 for 24 h, allowing the cells to attach the bottom of wells. After this period, these cells are treated with a closed up concentration to IC_{50} of other literature (serial dilution of free DOX, free nanocarrier and DOX-nanocarrier). There is a control group without treatment. After 24 h incubation, the solutions in microplate are removed, and the wells are washed with PBS. 20 μl MTT solution and 180 μl growth medium with 10% FBS are added to each well. After the incubation for an additional 4 h, the medium containing unreacted MTT is precisely removed from each well. To dissolve the formazan crystals, 150 μl of DMSO is added to each well. The absorbance of solubilized formazan is determined by ELISA plate reader at 570 nm which is followed by the evaluation of growth inhibition. All tests are conducted in triplicate. The cell viability percentages are calculated in the following formula:

$$\text{Cell viability } (\%) = \frac{\text{The absorbance of each test}}{\text{Mean absorbance of controls}} \times 100$$

2.8. Cellular uptake assay

Cellular uptake test with flow cytometry and fluorescence microscopy are performed to evaluate the quantitative and qualitative intracellular uptake amount of free DOX and DOX-nanocarrier into the cell. Due to the fluorescence feature DOX, another marker to view the cellular uptake process has not been used.

Cellular uptake with fluorescence microscopy: Approximately 20×10^3 Saos-2 cells are seeded in slide champers well. After incubation for 24 h, cells are treated with free DOX and DOX-nanocarrier at a concentration of IC_{50}. After the treatment of cells for 2–4 h, they are washed with PBS and observed with fluorescence microscopy (Olympus microscope Bh2-RFCA, Japan).

Cellular uptake with flow-cytometry: Saos-2 cells (500×10^3 cells per well) are seeded in a six-well and incubated for 24 h, then treated with free DOX, nanocarrier and DOX-nanocarrier in a concentration of IC_{50}. Cells with no treatment are considered as a negative control. After treatment for 2 and 4 h, cells are washed with PBS and observed with FACScalibur flow-cytometer to determine the fluorescent intensity related to DOX uptake inside the cells.

2.9. Apoptosis assay with DAPI staining

In order to evaluate the cellular apoptosis by observing the condensed and fragmented nuclei of cells, DAPI staining is used for the qualitative evaluation of apoptosis. Saos-2 cells (20×10^3 cells per well) are seeded on a slide chamber and incubated for 24 h, then treated by IC_{50} concentration of nanocarrier, free DOX, and DOX-nanocarrier. After 24 h, cells are washed with fresh PBS to remove any treated samples. Afterwards, cells are stained with 300 ng mL^{-1} DAPI solution for 15 min. DNA condensation and fragmentation in apoptotic cells are evaluated under fluorescence microscopy (Olympus microscope Bh2-RFCA, Japan). All experiments are performed in triplicate [15].

2.10. Apoptosis assay with flow-cytometry

To evaluate the cell apoptosis, Saos-2 cells (5×10^5 cells per well) are seeded in six-well with 10% growth medium. After the incubation for 24 h, cell culture media are replaced with fresh media and treated with nanocarrier, free DOX, and DOX-nanocarrier in a concentration of IC_{50} which is followed by the incubation of cells for 24 h. Cells are detached with trypsin and collected with centrifugation. Collected cells are washed with PBS and binding buffer to remove all trypsin. One million cells are suspended in 1 mL annexin binding buffer. To stain the apoptotic cell, a FITC-Annexin V apoptosis detection kit is used according to the manufacture's protocol as follow: 100 μL cell suspension, 5 μL FITCAnnexin V and 5 μL PI (propidium iodide) are mixed. Cells are incubated for 15 min and then 400 μL of binding buffer is added to each suspension. Finally, a FACS Calibur flow cytometer is used for analyzing the apoptotic cells.

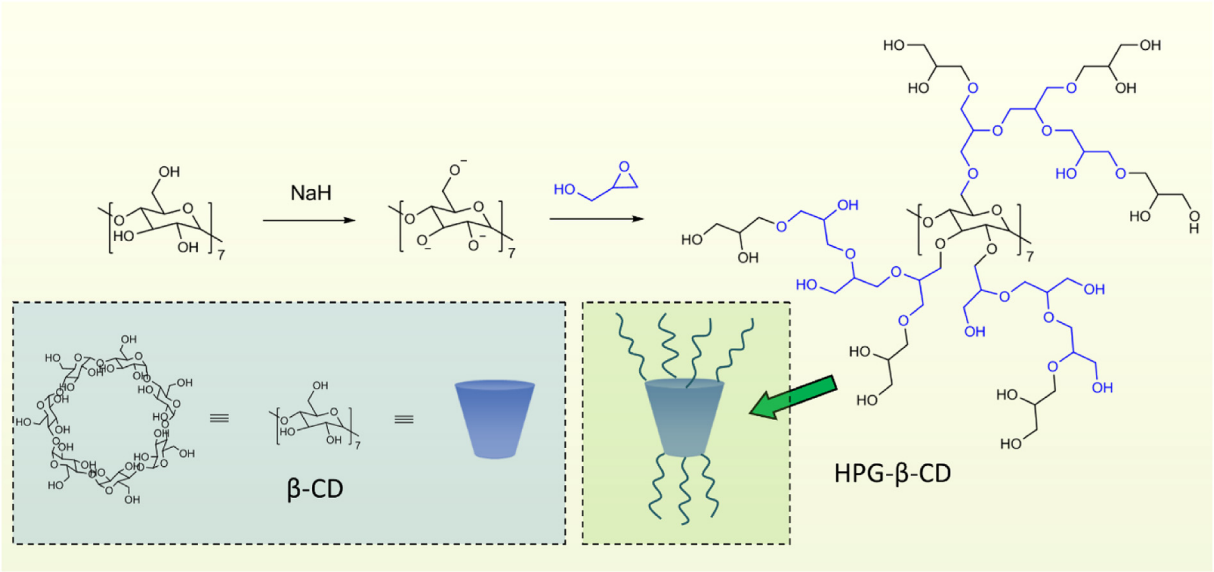

Fig. 1. Preparation process of hyperbranched polyglycerol modified β-cyclodextrin (HPG-β-CD).

3. Results and discussion

3.1. Preparation of magnetic nanocarrier

Magnetic nanocarrier based on hyper branched β-cyclodextrin is prepared according to the experimental section, as mentioned above. To clarify the reaction process and mechanisms, each step is orderly examined. Firstly, the hydroxyl functional groups (-OH) of β-cyclodextrin are activated by NaH reagent to create active nucleophile sties ($-O^-$) for opening glycidol rings via ring-opening polymerization reaction in the second step. Glycidol is reacted with active terminal sites to initiate the polymerization reaction. The resulting hyperbranched polyglycerol modified β-cyclodextrin (HPG-β-CD) has adequate proper functional groups for loading DOX as an anticancer agent (Fig. 1). Finally, magnetic nanoparticles (Fe_3O_4 NPs) are linked to HPG-β-CD in the presence of epichlorohydrin to obtain HPG-β-CD/Fe_3O_4 NPs as a magnetic nanocarrier.

3.2. Characterizations

After preparation of several characterizations (including FTIR, ^{1}H NMR, XRD, SEM, EDX, TEM, and DLS) were done to monitor and validate our reaction process. Each analysis was discussed separately, as well.

3.2.1. FTIR spectra

The chemical structure and functional group of each synthesized sample are evaluated by FTIR spectroscopy. Fig. 2 shows FTIR spectra of β-CD (a), HPG-β-CD (b), and HPG-β-CD/Fe_3O_4 NPs (c). One of the characteristic peaks of β-CD with broad and high intensity is appeared at 3380 cm^{-1} corresponded to O–H stretching vibration, while the vibration of CH and $–CH_2$- groups in β-CD structure is appeared in 2840–2930 cm^{-1} region. Due to the presence of C–O bonds in β-CD, a peak at 1161 cm^{-1} is also observed (Fig. 2a). Owing to the polymerization of glycerol on the surface of β-CD, no new peak is appeared and only some characteristic peaks including C–O, C–H and O–H are enhanced compared to β-CD. Thus, the presence of polymeric network on the surface of HPG-β-CD changes the characteristic peaks intensity at the mentioned area (1161, 2925, and 3380 cm^{-1}) (Fig. 2b). The FTIR spectrum of HPG-β-CD/Fe_3O_4 NPs shows a relatively moderate peak at 580 cm^{-1} corresponded to F–O bond and confirming the preparation magnetic nanoparticles (Fig. 2c).

3.2.2. NMR spectrometry

NMR spectroscopy are also used for validation of preparation process. NMR spectra of β-CD (a) and HPG-β-CD (b) and their characteristic peaks with regions are illustrated (Fig. 3). All the hydrogen (H2–H6) presented in β-CD are overlapped with a signal proton peak of HPG's methylene and methane. However, the signals of protons from H1 of β-CD is appeared around 4.8–5.2 ppm. Thus, the NMR results have totally confirmed and validated the grafting polymeric network of polyglycerol on β-CD to yield HPG-β-CD.

3.2.3. XRD analysis

XRD is a technique used to determine the atomic and molecular structure of a sample. The crystalline structure of β-CD (a) and HPG-β-CD (b) are evaluated by XRD analysis (Fig. 4). A series of sharp and intense diffraction peaks are appeared for β-CD while indicating its crystalline characteristic property. Its characteristic peaks are observed at 2θ around 6.4, 9.5, 11.0, 12.7, 13.5, 16.8, 18.2, 18.5, and 19.1°. The XRD analysis of HPG-β-CD has shown that the surface modification of β-CD has been successfully performed because the crystalline structure is significantly changed. No sharp and intense peaks are observed for HPG-β-CD, however, there are only two broad peaks at 10 and 35°.

3.2.4. SEM and EDX analysis

SEM produces the images of a samples by scanning the surface with a focused beam of electrons. The surface morphology of β-CD (a), HPG-β-CD (b), and HPG-β-CD/Fe_3O_4 NPs (c) as a magnetic nanocarrier have been evaluated by SEM analysis (Fig. 5). The result has shown that the size of β-CD is reported 10 μm with relatively smooth. Regarding the several areas of this sample, there are some crystalline structures, causing intense peaks in XRD diffraction. After the surface modification of β-CD with ring polymerization of glycidol, the surface of sample is specifically altered to rough and branched like structure which clearly observed at the surface of HPG-β-CD. Finally, the synthesized Fe_3O_4 NPs is modified with HPG-β-CD to create the spherical particles in size of 30 nm. By using Energy-dispersive, X-ray spectroscopy estimates the percentage of different elements in β-CD (a), HPG-β-CD (b), and HPG-β-CD/Fe_3O_4 NPs (c). The results have shown that β-CD consists of two main elements of C and O with a weight of 80% and 20%. After the surface modifying of β-CD with glycidol, atomic percentage of C and O is changed to 55.3% and 44.7%, respectively. Finally, decorating magnetic nanoparticles (Fe_3O_4 NPs) changes the percentage of elements to 31.40%, 18.5% and 50.1% for C, O and Fe, respectively.

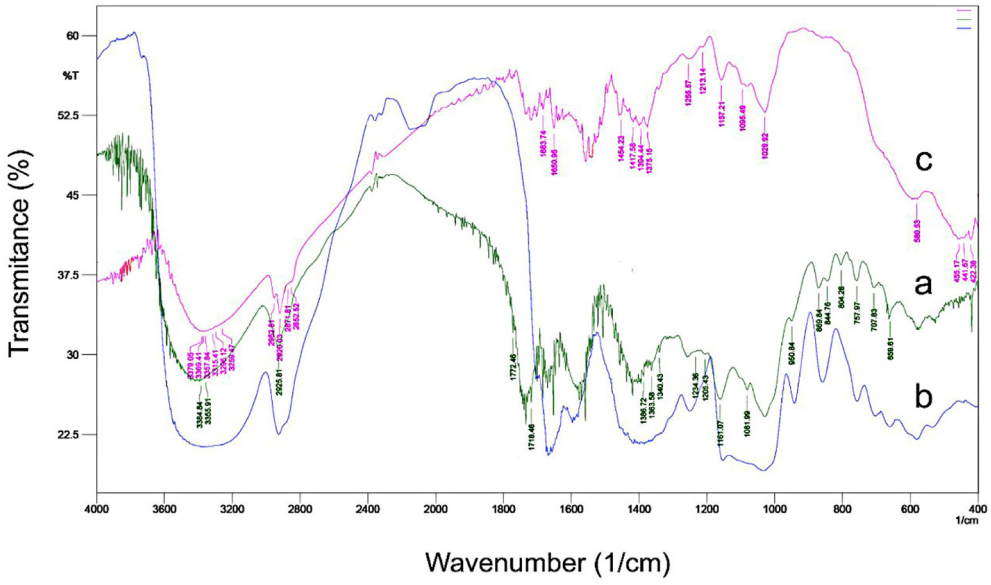

Fig. 2. The FTIR spectra of β-CD (a), HPG-β-CD (b), and HPG-β-CD/Fe_3O_4 NPs (c).

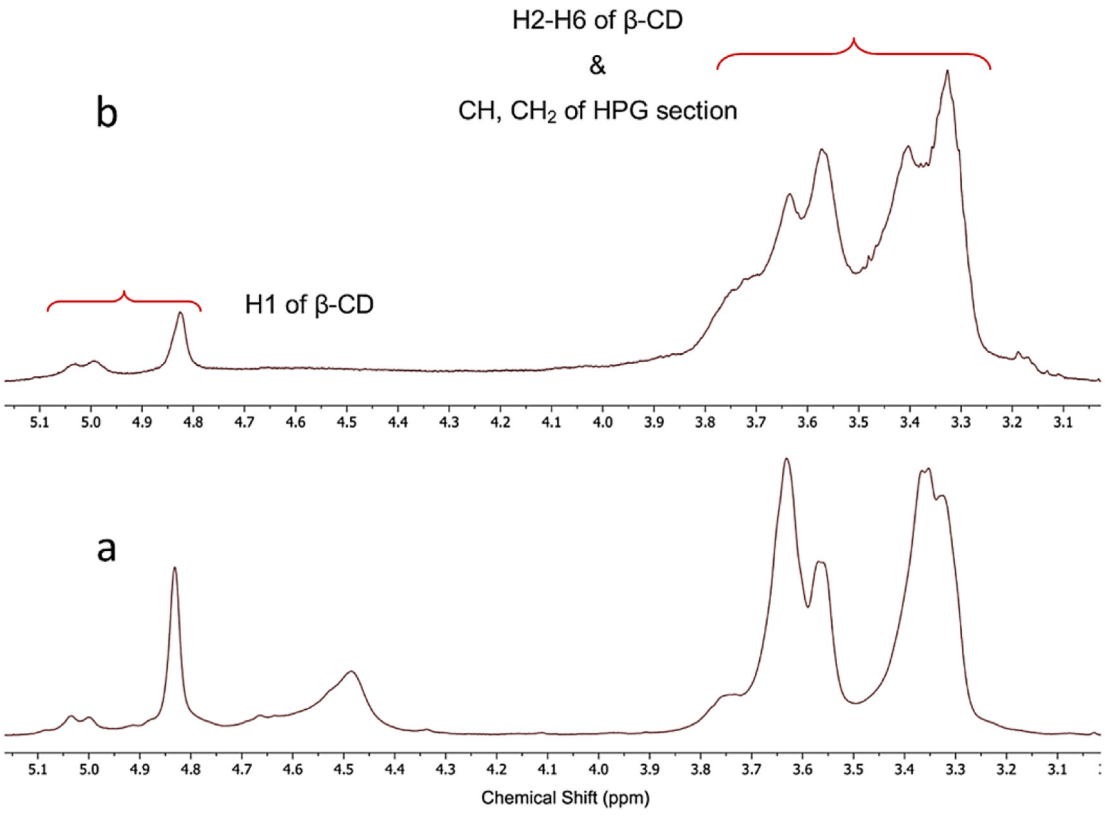

Fig. 3. The HNMR spectra of β-CD (a) and HPG-β-CD (b) in deuterated DMSO.

3.2.5. TEM analysis

In order to investigate the size and morphology of nanoparticles, a TEM imaging analysis has been used. Accordingly, the size of nanocarrier is approximately estimated to 50 nm (Fig. 6). Also, the spherical structure of nanoparticle is obviously visible. By Zooming the TEM images, its observed that nanoparticles have a core-shell structure. Therefore, it can be found that magnetic nanoparticles are located in the central core and surrounded by a layer of polymer in the shell (see Fig. 7).

3.2.6. DLS technique and zeta potential

Although the size of magnetic nanocarrier (HPG-β-CD/Fe_3O_4 NPs) is observed and calculated by SEM analysis. Particle size can be determined by measuring the random changes in the intensity of light scattered from a suspension. DLS is a technique that can be used to the purpose of determining ingredient scattering of the samples. DLS result has indicated that the hydrodynamic particle size is 14.86 nm which is similar to the result of SEM and TEM. The surface charge of magnetic nanocarrier in PBS solution (physiological condition; pH = 7.4) is also determined. The result has shown that total charge on sample is −35

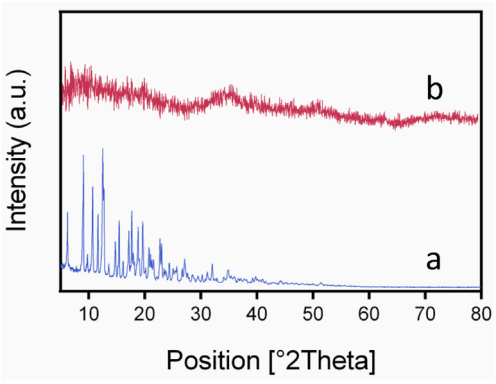

Fig. 4. XRD diffraction of β-CD (a) and HPG-β-CD (b) at 2Theta (2θ) range of 5–80°.

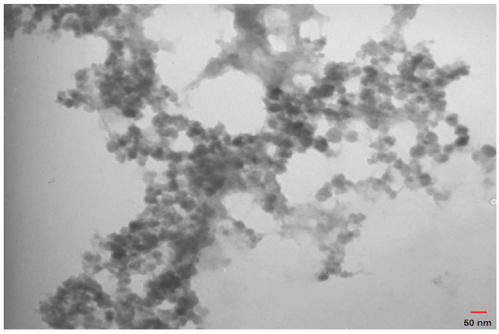

Fig. 6. TEM analysis of HPG-β-CD/Fe_3O_4 NPs with core-shell structure.

mV. This is because of the presence of high content of hydroxyl groups at the surface of platform.

3.3. In vitro DOX loading and release study

Doxorubicin (DOX) is an anticancer drug that well soluble in PBS that is properly connected to nanocarrier in loading condition. The electrostatic bonds between the functional group of nanocarrier and DOX has made an effective connection. In addition, the presence of branches and cavities in HPG-β-CD could be the reason(s) of DOX loading. After incubation for 24 h in dark condition, DOX is loaded on nanocarrier and unloaded DOX could be removed from the surface of nanocarrier with the help of an external magnet and several washing steps. The supernatant is separated and their optical density has been measured. According to the results, the encapsulation and loading efficiencies of DOX are 98% and 9.8%, respectively. In order to study the pH responsiveness ability of DOX-nanocarrier, *in-vitro* release study is

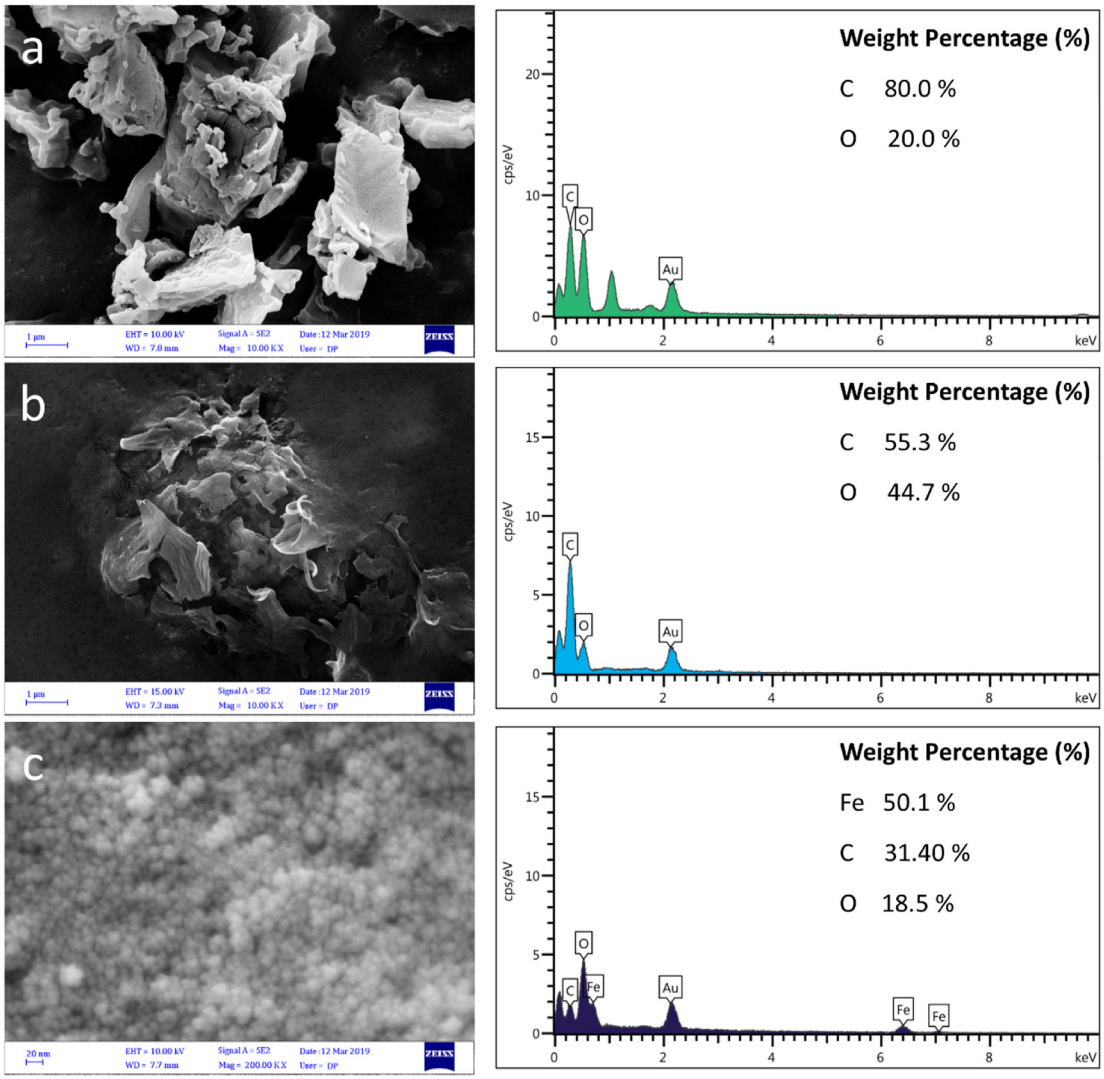

Fig. 5. The SEM and EDX analysis of β-CD (a), HPG-β-CD (b), and HPG-β-CD/Fe_3O_4 NPs (c).

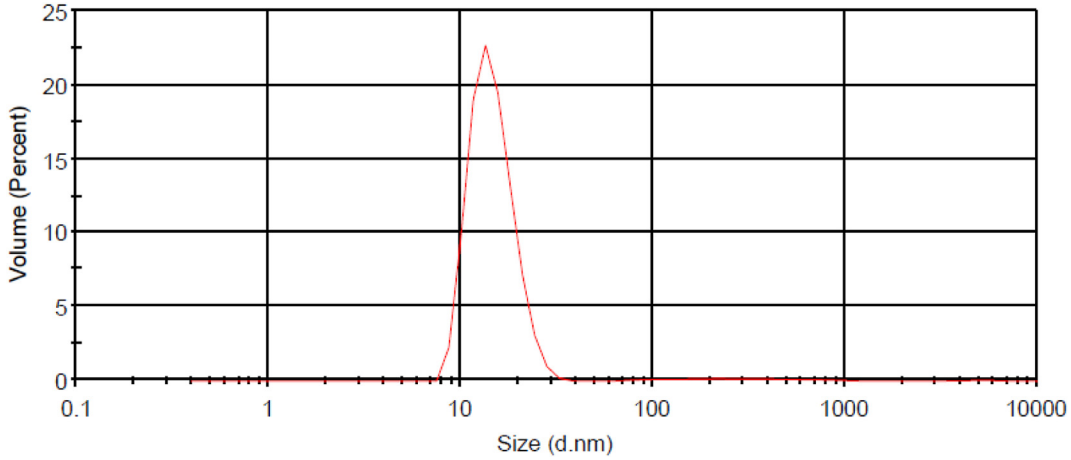

Fig. 7. DLS technique for analyzing the size distribution of HPG-β-CD/Fe_3O_4 NPs in physiological condition (pH 7.4).

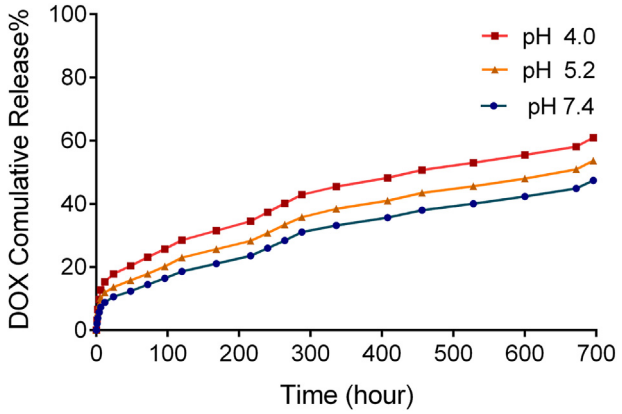

Fig. 8. Cumulative release of DOX at various pH values (4, 5.2, and 7.4) at 37 °C.

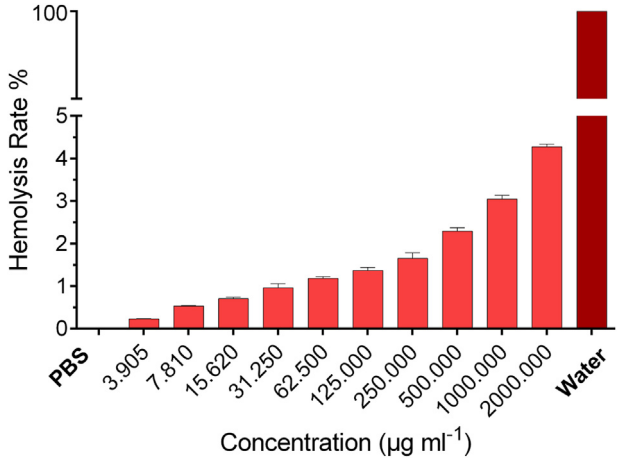

Fig. 9. Hemolysis rate of HRBCs in the presence of nanocarrier at different concentrations (negative control: PBS, positive control: water).

performed. For this purpose, various conditions have been chosen such as lysozyme, tumor microenvironment and healthy tissue condition by using different pH values as 4, 5.2 and 7.4 at 37°, respectively. After 29 days, the results have shown that 60%, 53%, and %47 of DOX are released from nanocarrier at pH 4, 5.2 and 7.4, respectively (Fig. 8). Additionally, the graphs have indicated that a burst release, during the first 48 h, is reached to 20%, 15%, and 12% at pH 4, 5.2 and 7, respectively. The first severe release is due to the dissemination of the surface-bound and physically adsorbed drug molecules on the surface of nanocarrier. Therefore, it can be concluded that the prepared nanoparticles under acidic conditions of tumor microenvironment and lysozyme have more and faster release than the healthy tissues. The pH-dependent release of DOX from HPG-β-CD/Fe_3O_4 NPs might be essentially due to the change of hydrogen bonding interaction between β-CD and DOX (see Fig. 9).

At pH 7.4, several robust hydrogen-bonding interactions have been occurred between O, H atoms and NH2–, OH– groups which can inhibit the drug release. However, in lower pH such as 4 and 5.2, a higher degree of protonation has weaken the hydrogen bonds and has released the drug from the nanoparticles [47].

3.4. Biocompatibility evaluation of magnetic nanocarrier

In order to study the biocompatibility of nanocarrier, the effects of nanocarrier on the membrane of human RBCs are evaluated by using the hemolysis assay test. In this regard, different concentrations of nanocarrier (2000–3.905 μg mL^{-1}) interact with RBCs. The optical density of supernatant has been measured at 540 nm by using UV–vis spectroscopy. The hemolysis rates are listed in Table 1 for each experimental group. The results have indicated that even at high concentrations of nanocarrier, negligible hemolytic effects have been observed under physiological condition. Also, the results are compared with negative (PBS) and positive (distilled water) control group with a hemolysis rate of 0% and 100%, respectively. Results have verified the compatibility and accommodation of nanocarrier with RBCs while proposed that nanocarrier is a suitable drug delivery system for *in vivo* applications.

Table 1
Hemolysis test of nanocarrier at different concentration.

Sample Conc. (ppm)	PBS	3.90	7.81	15.62	31.25	62.5	125	250	500	1000	2000	Water
Hemolysis Rate (%)	0	0.22	0.32	0.71	0.96	1.68	1.37	1.65	2.29	3.04	4.27	100

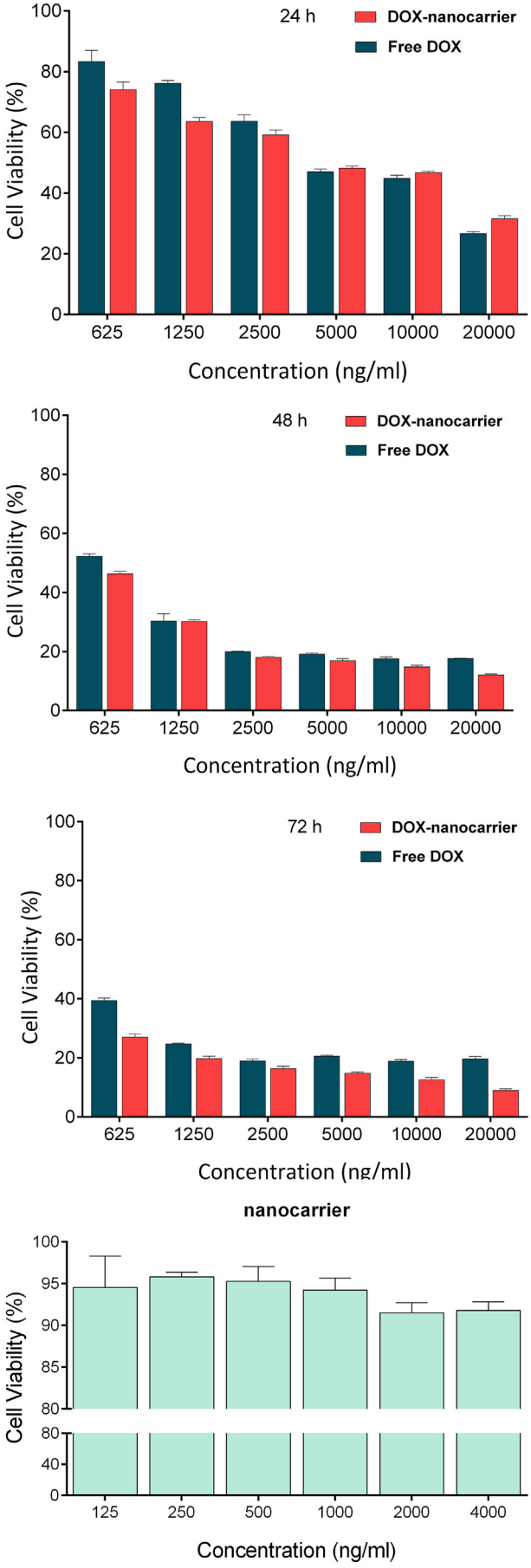

Fig. 10. Cell growth inhibition rate by different concentration of free DOX, DOX-nanocarrier and free nanocarrier after 24, 48 and 72 h.

3.5. *In-vitro cytotoxicity assay by MTT assay*

In-vitro cellular cytotoxicity studies of free DOX, nanocarrier and DOX-nanocarrier have been evaluated by MTT assay for 24, 48 and 72 h (Fig. 10). The cytotoxic effect of nanocarrier on Saos-2 cell line has shown no toxicity even in high concentration (20,000 ng mL^{-1}) of nanocarrier with absolutely cells survived (IC_{50} ~ no reached). These results have shown that nanocarrier is safe and biocompatible for using drug delivery systems. To compare the toxicity and survival rate of free DOX and DOX-nanocarrier, cell is treated with different concentration. The IC_{50} values of free DOX after 24, 48 and 72 h are reported as 5554, 465.5 and 235.6 ng mL^{-1}, respectively. Also, the IC_{50} values of DOX that loads nanocarrier after 24, 48 and 72 h are reported 5057, 399.5 and 143.3 ng mL^{-1},respectively. After 24 h, cytotoxic effects of drug-nanocarrier on Saos-2 cells have not been well characterized and drug-nanocarrier are less toxic than free drugs. However, 48 and 72 h after treatment, the cytotoxic eff ects of drug-nanocarrier have been improved and IC_{50} is reduced, resulting that cell cytotoxicity of DOX-nanocarrier and free DOX are time dependent and IC_{50} rate is decreased over the time.

3.6. *Cellular uptake assay*

The quantitative and qualitative cellular uptake test has been conducted to determine the amount of internalization of DOX-nanocarrier in Saos-2 cells. A qualitative evaluation has been performed with fluorescence microscopy (Fig. 11). The internalization rate of Saos-2 cells shows that a significant amount of DOX-nanocarrier is uptake by saos-2 cells. The results have confirmed that the uptake process is completed at first 1 h. A quantitative evaluation is also performed with flow cytometry at. Based on Fig. 12, 99.4% of DOX-nanocarrier is uptake by Saos-2 cells after 1 h.

3.7. *Apoptosis assay with DAPI staining*

DAPI staining is a type of nucleus coloration which can be used to evaluate the nuclei morphology of the cells. In this technique, with the help of fluorescent microscopy, after treatment of Saos-2 cell for 24 h with free DOX, free nanocarrier and DOX-nanocarrier, the condition of apoptosis and necrosis of the cells are investigated and compared with control group. Accordingly, no evidence of apoptosis and necrosis in untreated control Saos-2 cells (a) and Saos-2 cells treated with nanocarrier (b) has been observed (Fig. 13). The nuclear morphology of these groups is quite similar without showing significant chromatin degradation. Whereas, the nucleus morphology of treated cells with free DOX (c) and DOX-nanocarrier (d) has many changes and the symptoms of apoptosis are well visible within the nuclei. Evidence such as shrinkage, fragmentation and perforation of nucleus is well observed in cells. Nevertheless, under the same time and almost nearly concentration, highly fragmented nuclei are observed in DOX-nanocarrier versus free DOX. Therefore, in this study, it is conducted that DOX-nanocarrier is a suitable target therapy for apoptosis of cancerous Saos-2 cells and a better inhibitor for Saos-2 cell growth than free DOX.

3.8. *Apoptosis assay with flow-cytometry*

In order to evaluate the apoptosis rate of saos-2 cells, cells after treatment with free DOX, free nanocarrier and DOX-nanocarrier for 48 h are stained with annexin V and PI. Those cells without treatment are considered as control group. The flow-cytometry results have shown that those cells treated with free nanocarrier have no apoptotic effects. Absence of apoptotic effects of nanocarrier on cancer cells has indicated

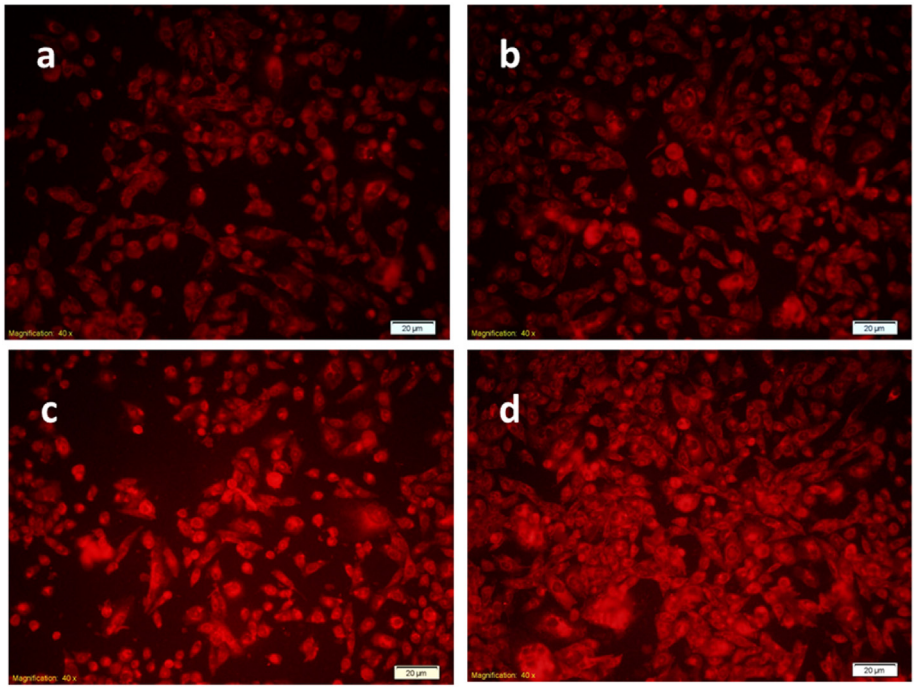

Fig. 11. DOX loaded nanocarrier uptake by Saos-2 cells for 1 (a), 2 (b), 3 (c), 4 (d) hour.

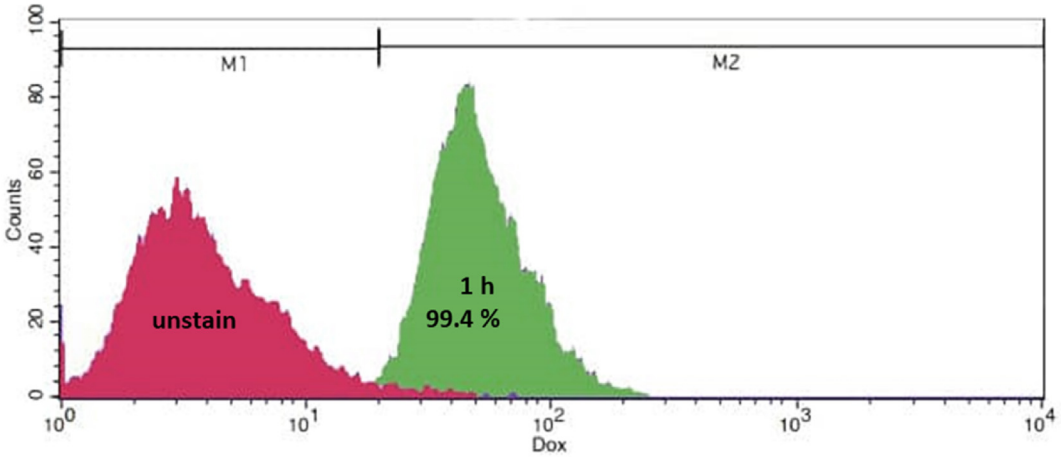

Fig. 12. Cellular uptake percentage of DOX-nanocarrier by Saos-2 cells 1 h after treatment.

that nanocarrier are non-toxic. In contrast, drug treated with free DOX and DOX-nanocarrier are significantly apoptotic (Fig. 14). In the same concentration of drug, it is observed that the apoptotic effect of DOX-nanocarrier is more than free DOX.

4. Conclusion

In this study, smart hyper-branched magnetic nanocarrier with a core-shell structure, biocompatible and pH-sensitive character have been designed. Due to the presence of abundant functional hydroxyl groups, branched structure of polyglysidol at the surface of β-cyclodextrin and holes in beta-cyclodextrin structure, drug loading of nanocarrier is appropriate. In-vitro release study has shown that nanocarrier has a pH responsive character. The effects of these drug delivery systems on Saos-2 cell line have been evaluated. Thus, the results of cytotoxicity assay have shown that toxicity of drug-loaded nanocarrier in 48 h and 72 h after treatment is higher than free DOX. The results of cellular uptake assay with both fluorescent microscopy and flow cytometry confirm that suitable amount of nanocarrier is harvested by the cells during the early hours. DAPI staining and apoptosis study in 48 h by flow cytometry confirm that DOX-nanocarrier has more apoptotic effect than free DOX. It can be concluded that the use of this smart nanocarrier system can be effectively used in treatment of bone cancer such as osteosarcoma.

CRediT authorship contribution statement

Nafiseh Khelghati: Formal analysis, Investigation, Writing - original draft. **Yousef Rasmi:** Supervision. **Navid Farahmandan:** Formal analysis. **Alireza Sadeghpour:** Formal analysis. **Seyed Mostafa Mir:** Methodology. **Ansar Karimian:** Methodology. **Bahman Yousefi:** Formal analysis.

Acknowledgements

The Authors would like to thanks Clinical Research Development Unit, Shohada Hospital, Tabriz University of Medicl Sciences for kind supports.

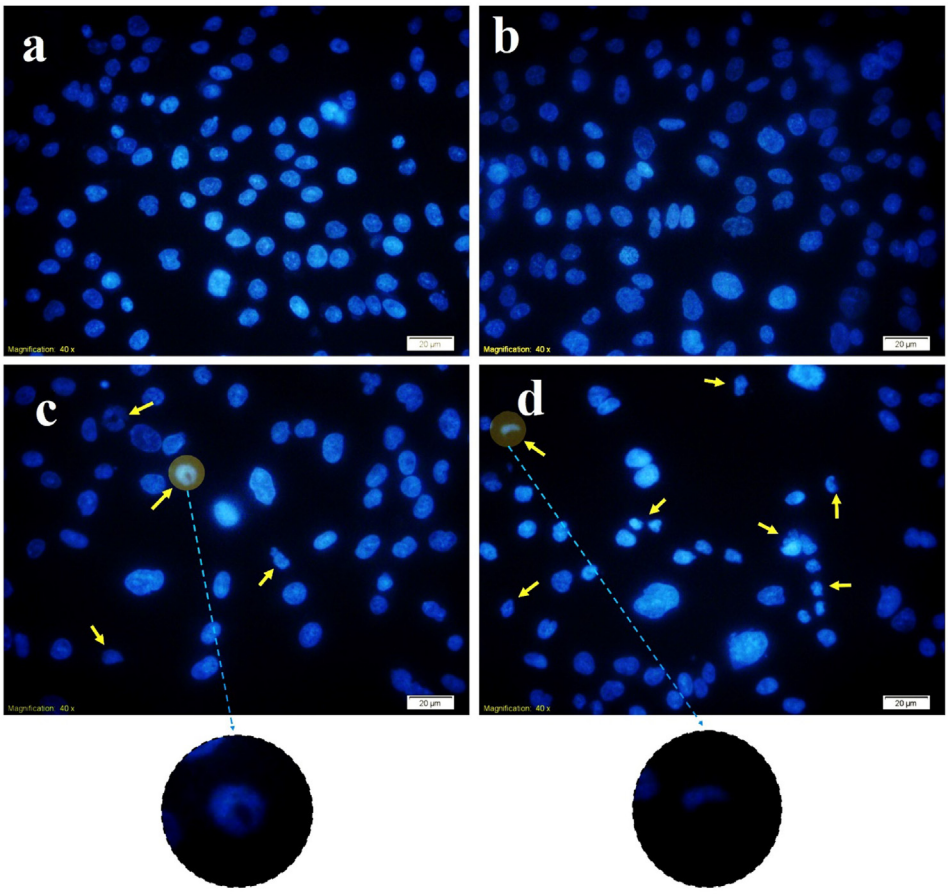

Fig. 13. DAPI staining of negative control (a), nanocarrier (b), free DOX (c), and DOX-nanocarrier (d).

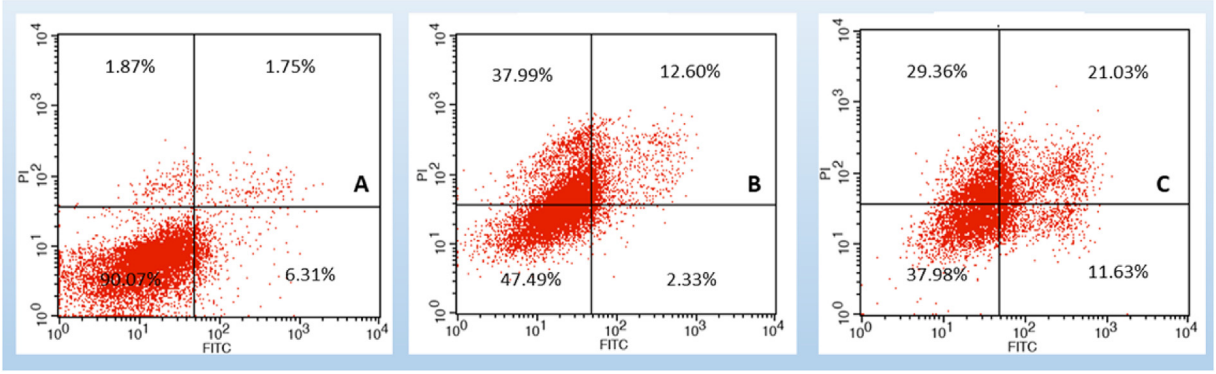

Fig. 14. Apoptotic effect of Saos-2 cell line by flow cytometry for nanocarrier (A), free DOX (B), DOX-nanocarrier (C).

Appendix A. Supplementary data

Supplementary data to this article can be found online at https://doi.org/10.1016/j.jddst.2020.101741.

References

[1] G.B.o.D.C. Collaboration, Global, regional, and national cancer incidence, mortality, years of life lost, years lived with disability, and disability-adjusted life-years for 29 cancer groups, 1990 to 2017: a systematic analysis for the global burden of disease study, JAMA Oncology (2019), https://doi.org/10.1001/jamaoncol.2019.2996.

[2] C.E. DeSantis, et al., Cancer treatment and survivorship statistics, 2014, CA A Cancer J. Clin. 64 (4) (2014) 252–271.

[3] M. Rahimi, et al., Highly branched amine-functionalized p-sulfonatocalix [4] arene decorated with human plasma proteins as a smart, targeted, and stealthy nanovehicle for the combination chemotherapy of MCF7 cells, New J. Chem. 42 (15) (2018) 13010–13024.

[4] A. Luetke, et al., Osteosarcoma treatment–where do we stand? A state of the art review, Canc. Treat Rev. 40 (4) (2014) 523–532.

[5] G. Ottaviani, N. Jaffe, The epidemiology of osteosarcoma, Pediatric and Adolescent Osteosarcoma, Springer, 2009, pp. 3–13.

[6] K.A. Janeway, R. Maki, T.F. DeLaney, Chemotherapy and Radiation Therapy in the Management of Osteosarcoma, UpToDate, 2018.

[7] Z. Liao, et al., Outcomes of surgery and/or combination chemotherapy for extraskeletal osteosarcoma: a single-center retrospective study from China, Sci. Rep. 9 (1) (2019) 4816.

[8] S.M. Blaney, M.A. Smith, J.L. Grem, Doxorubicin: role in the treatment of osteosarcoma, Osteosarcoma in Adolescents and Young Adults: New Developments and Controversies, Springer, 1993, pp. 55–73.

[9] O. Tacar, P. Sriamornsak, C.R. Dass, Doxorubicin: an update on anticancer molecular action, toxicity and novel drug delivery systems, J. Pharm. Pharmacol. 65 (2) (2013) 157–170.

[10] V. Shafiei-Irannejad, et al., Reversion of multidrug resistance by co-encapsulation of doxorubicin and metformin in poly (lactide-co-glycolide)-d-α-tocopheryl polyethylene glycol 1000 succinate nanoparticles, Pharmaceut. Res. 35 (6) (2018) 119.

[11] M. Mobaraki, et al., Molecular mechanisms of cardiotoxicity: a review on major side-effect of doxorubicin, Indian J. Pharmaceut. Sci. 79 (3) (2017) 335–344.
[12] O.J. Arola, et al., Acute doxorubicin cardiotoxicity involves cardiomyocyte apoptosis, Canc. Res. 60 (7) (2000) 1789–1792.
[13] F. Zolfagharzadeh, V.D. Roshan, Pretreatment hepatoprotective effect of regular aerobic training against hepatic toxicity induced by doxorubicin in rats, Asian Pac. J. Cancer Prev. APJCP 14 (5) (2013) 2931–2936.
[14] B. Haley, E. Frenkel, Nanoparticles for drug delivery in cancer treatment, Urologic Oncology: Seminars and Original Investigations, Elsevier, 2008.
[15] M. Rahimi, et al., Dendritic chitosan as a magnetic and biocompatible nanocarrier for the simultaneous delivery of doxorubicin and methotrexate to MCF-7 cell line, New J. Chem. 41 (8) (2017) 3177–3189.
[16] A. Karimian, H. Parsian, M. Majidinia, M. Rahimi, S.M. Mir, H. Samadi Kafil, V. Shafiei-Irannejad, M. Kheyrollah, H. Ostadi, B. Yousefi, Int. J. Biol Macromol. 15 (133) (2019) 850–859.
[17] X. Sun, et al., Bone-targeting drug delivery system of biomineral-binding liposomes loaded with icariin enhances the treatment for osteoporosis, J. Nanobiotechnol. 17 (1) (2019) 10.
[18] A.P.P. Kröger, et al., Biocompatible single-chain polymer nanoparticles for drug delivery—a dual approach, ACS Appl. Mater. Interfaces 10 (37) (2018) 30946–30951.
[19] M. Rahimi, et al., Multi-branched ionic liquid-chitosan as a smart and biocompatible nano-vehicle for combination chemotherapy with stealth and targeted properties, Carbohydr. Polym. 196 (2018) 299–312.
[20] M. Rahimi, et al., Needle-shaped amphoteric calix [4] arene as a magnetic nanocarrier for simultaneous delivery of anticancer drugs to the breast cancer cells, Int. J. Nanomed. 14 (2019) 2619.
[21] M.V. Braham, et al., Liposomal drug delivery in an in vitro 3D bone marrow model for multiple myeloma, Int. J. Nanomed. 13 (2018) 8105.
[22] I. Villamagna, et al., Preparation of a novel intra-articular polymeric drug delivery system, Osteoarthritis Cartilage 26 (2018) S286.
[23] G. Marcelo, et al., Development of itaconic acid-based molecular imprinted polymers using supercritical fluid technology for pH-triggered drug delivery, Int. J. Pharm. 542 (1–2) (2018) 125–131.
[24] B. Sun, et al., Disulfide bond-driven oxidation-and reduction-responsive prodrug nanoassemblies for cancer therapy, Nano Lett. 18 (6) (2018) 3643–3650.
[25] E. Jooybar, et al., Enzymatically crosslinked hyaluronic acid microgels as a vehicle for sustained delivery of cationic proteins, Eur. Polym. J. 115 (2019) 234–243.
[26] M. Rahimi, et al., A novel bioactive quaternized chitosan and its silver-containing nanocomposites as a potent antimicrobial wound dressing: structural and biological properties, Mater. Sci. Eng. C 101 (2019) 360–369.
[27] M.G. Mehrabani, et al., Chitin/silk fibroin/TiO2 bio-nanocomposite as a biocompatible wound dressing bandage with strong antimicrobial activity, Int. J. Biol. Macromol. 116 (2018) 966–976.
[28] M.-E. Kyriazi, et al., Multiplexed mRNA sensing and combinatorial-targeted drug delivery using DNA-gold nanoparticle dimers, ACS Nano 12 (4) (2018) 3333–3340.
[29] N.A.B. Ghazali, M.P. Mani, S.K. Jaganathan, Green-synthesized zinc oxide nanoparticles decorated nanofibrous polyurethane mesh loaded with virgin coconut oil for tissue engineering application, Curr. Nanosci. 14 (4) (2018) 280–289.
[30] X.-H. Peng, et al., Targeted magnetic iron oxide nanoparticles for tumor imaging and therapy, Int. J. Nanomed. 3 (3) (2008) 311.
[31] K. El-Boubbou, Magnetic iron oxide nanoparticles as drug carriers: clinical relevance, Nanomedicine 13 (8) (2018) 953–971.
[32] K. El-Boubbou, Magnetic iron oxide nanoparticles as drug carriers: preparation, conjugation and delivery, Nanomedicine 13 (8) (2018) 929–952.
[33] N. Tran, T.J. Webster, Magnetic nanoparticles: biomedical applications and challenges, J. Mater. Chem. 20 (40) (2010) 8760–8767.
[34] A. Hajinasab, et al., Preparation and characterization of a biocompatible magnetic scaffold for biomedical engineering, Mater. Chem. Phys. 204 (2018) 378–387.
[35] V.F. Cardoso, et al., Advances in magnetic nanoparticles for biomedical applications, Adv. Healthcare Mater. 7 (5) (2018) 1700845.
[36] M. Prabaharan, J. Mano, Chitosan derivatives bearing cyclodextrin cavitiesas novel adsorbent matrices, Carbohydr. Polym. 63 (2) (2006) 153–166.
[37] E. Merisko-Liversidge, G.G. Liversidge, E.R. Cooper, Nanosizing: a formulation approach for poorly-water-soluble compounds, Eur. J. Pharmaceut. Sci. 18 (2) (2003) 113–120.
[38] M.E. Davis, M.E. Brewster, Cyclodextrin-based pharmaceutics: past, present and future, Nat. Rev. Drug Discov. 3 (12) (2004) 1023.
[39] K.C.-F. Leung, K.-N. Lau, Self-assembly and thermodynamic synthesis of rotaxane dendrimers and related structures, Polym. Chem. 1 (7) (2010) 988–1000.
[40] J.P. Gunning, et al., The development of poly (dendrimer) s for advanced processing, Polym. Chem. 1 (5) (2010) 730–738.
[41] G.K. Kouassi, J. Irudayaraj, A nanoparticle-based immobilization assay for prion-kinetics study, J. Nanobiotechnol. 4 (1) (2006) 8.
[42] A.A. Nada, et al., Cellulose-based click-scaffolds: synthesis, characterization and biofabrications, Carbohydr. Polym. 199 (2018) 610–618.
[43] Y. Xue, et al., Amphoteric calix [8] arene-based complex for pH-triggered drug delivery, Colloids Surf. B Biointerfaces 101 (2013) 55–60.
[44] M. Rahimi, K.D. Safa, R. Salehi, Co-delivery of doxorubicin and methotrexate by dendritic chitosan-g-mPEG as a magnetic nanocarrier for multi-drug delivery in combination chemotherapy, Polym. Chem. 8 (47) (2017) 7333–7350.
[45] C. Du, et al., A pH-sensitive doxorubicin prodrug based on folate-conjugated BSA for tumor-targeted drug delivery, Biomaterials 34 (12) (2013) 3087–3097.
[46] M. Rahimi, et al., Biocompatible magnetic tris (2-aminoethyl) amine functionalized nanocrystalline cellulose as a novel nanocarrier for anticancer drug delivery of methotrexate, New J. Chem. 41 (5) (2017) 2160–2168.
[47] X. Fan, et al., Magnetic Fe 3 O 4–graphene composites as targeted drug nanocarriers for pH-activated release, Nanoscale 5 (3) (2013) 1143–1152.